PHYSICAL REVIEW B **100**, 214436 (2019)

Exchange bias and spin glass states driven by antisite disorder in the double perovskite compound $LaSrCoFeO_6$

R. C. Sahoo,[1,*] Y. Takeuchi,[2] A. Ohtomo,[2,3] and Z. Hossain[1,†]
[1]*Department of Physics, Indian Institute of Technology, Kanpur 208016, India*
[2]*Department of Chemical Science and Engineering, Tokyo Institute of Technology, 2-12-1 Ookayama, Meguro-ku, Tokyo 152-8552, Japan*
[3]*Materials Research Center for Element Strategy (MCES), Tokyo Institute of Technology, Yokohama 226−8503, Japan*

(Received 21 August 2019; revised manuscript received 3 December 2019; published 26 December 2019)

Antisite (B-site) disorder in double perovskite lattice is responsible for various magnetic phenomena such as exchange bias, spin glass, memory effect, colossal magnetoresistance, etc. By controlling the antisite disorder in the antiferromagnetic double perovskite $LaSrCoFeO_6$, we achieve intrinsic exchange bias effect with a large exchange bias field (∼1.2 kOe) and giant coercive field (∼12.8 kOe). Further, we find that the effect of such antisite disorder induces a spin-glass state in $LaSrCoFeO_6$. Multiple signatures of slow dynamics were confirmed by frequency-dependent peak shift, slow spin relaxation, and memory effect over a wide temperature regime (5−80 K). The AC susceptibility data near the spin-glass temperature ($\sim 72.1 \pm 0.6$ K) are best fit by a critical slowing down model described by a dynamical exponent $z\nu = 7.5 \pm 0.5$ and $\tau_0 = 1.05 \times 10^{-12}$ s. The origin of exchange bias and spin glass are briefly discussed.

DOI: 10.1103/PhysRevB.100.214436

I. INTRODUCTION

In recent times, there has been a lot of interest in three-dimensional (3D) double perovskite (DP) systems as they provide a rich material platform for studying emergent functionalities like near-room-temperature ferromagnetic (FM) insulators, magnetodielectrics, exchange bias (EB) anisotropy, magnetocaloric effects, colossal magnetoresistance, etc. [1–5]. These interesting phenomena emerge because of complex couplings between spin, charge, orbital, and lattice degrees of freedom in DPs [6,7]. All these multifunctional interesting features in DP systems have been made possible by introducing disorder into the system by partially substituting *A*-site and/or *B*-site elements in the DP structure ($A_{2-x}A'_xBB'O_6$, where A and A' are occupied by rare-/alkaline-earth and B and B' are occupied by *d* transition-metal elements) [8]. The synthesis of DP at high temperature also creates disorder in the crystal structure [5,6]. In most of the DP system, these two issues lead to distortion in corner-shared BO_6 and $B'O_6$ octahedra as well as partial antisite disorder ASD effect. Due to ASD, alternating BO_6 and $B'O_6$ octahedra are misplaced from their ordered position, which creates additional B-O-B or B′-O-B′ antisite couplings instead of B-O-B' spontaneous couplings [4,6,9]. The magnetic and transport properties are strongly influenced by these two structural factors: distorted crystal structure and ASD effect [5,10]. The ASD effect can be experimentally determined by the deviation of saturation magnetization M_S from the expected M_S of this system in the ordered phase. It can also be verified from Rietveld refinement and crystal structure data [10–12]. Moreover, recent studies on such systems have revealed that the coexistence of spontaneous and antisite couplings result in competing FM and antiferromagnetic (AFM) interactions, leading to magnetic frustration that suppresses FM long-range ordering [4,9,13]. For example, Murthy *et al.* reported that the coupling between FM and AFM phases increases with the increase of ASD because of doping at the trivalent rare-earth (La^{3+}) site by divalent alkaline-earth ions (Sr^{2+}) in $La_{2-x}Sr_xCoMnO_6$ ($0 \leqslant x \leqslant 1$) systems [6]. Also, Wang *et al.* stated that by modulating the synthesis temperature of La_2NiMnO_6 systems, one can control the ASD distribution in the sample and hence AFM coupling intensity can be manipulated accordingly [14].

Additionally, in these magnetic inhomogeneous systems, the interface anisotropy between frustrated FM and AFM phase boundary gives rise to EB effect along the FM magnetization direction [5,6]. The EB effect is described as a horizontal and/or vertical shift of the magnetic hysteresis loop. The EB materials have led to applications such as spin valves [15], permanent magnets [16], thermally assisted magnetic random access memories [17], and other spintronic devices [4–6,18]. Apart from the FM/AFM interface, EB effect has also been observed for FM/ferrimagnetic (FiM), FM/spin glass (SG), and AFM/SG interfaces. Materials with a large EB and coercive field are of great fundamental and technological interest to the scientific community. In these materials, the magnitude and sign of EB robustly depends on the direction and strength of the bias field as well as interface anisotropy. This agrees with the results obtained for La_2NiMnO_6 [14], $La_{1.5}Ca_{0.5}CoMnO_6$ [5], and $La_{2-x}Ca_xCoMnO_6$ [6] frustrated oxides.

In 1998, Ueda *et al.* [8] synthesized an artificial FM superlattice of $LaFeO_3$-$LaCrO_3$ by stacking alternate layers of AFM-$LaFeO_3$ and AFM-$LaCrO_3$ perovskites. This superlattice DP system exhibits FM ordering due to Cr^{3+}-O-Fe^{3+} long-range coupling, which follows the Goodenough-Kanamori 180° superexchange rule. Moreover, nonmagnetic

---

[*] rsahoo@iitk.ac.in
[†] zakir@iitk.ac.in

$LaCoO_3$ has been extensively studied for its metal-semiconductor transition as well as temperature-dependent spin-state transition of Co ($S = 0$, $S = 1$, and $S = 2$) [19–21]. Interestingly, the spin states and valence state of a Co ion in this system can be artificially manipulated by introducing Jahn-Teller distortion in the crystal structure as a result of hole doping at the La^{3+} site as reported in Refs. [22,23]. The low-temperature SG and high-temperature FM states are also observed due to the doping and/or thermally activated competing mechanism between Co-Co couplings [22]. The AFM-$SrFeO_3$ perovskite has also attracted continuing interest for decades due to its unusual physical properties like temperature-dependent giant negative magnetoresistance, Mott insulator, pressure-induced switching magnetism, multiple magnetic anomalies, and helical spin texture [24–26]. The interesting results from $LaFeO_3$-$LaCrO_3$ superlattice and renewed interest in $LaCoO_3$ and $SrFeO_3$ parent perovskites have motivated us to investigate the structural and magnetic properties in daughter $LaSrCoFeO_6$ (LSCFO = $LaCoO_3$ + $SrFeO_3$) DP.

It is known that ASD plays a crucial role in the structural and magnetic properties of DPs. Thus, understanding of structural and different magnetic interactions as a function of degrees of transition metal (Co and Fe) order in frustrated LSCFO DP is very important. In this paper, we have studied ASD-driven magnetism in frustrated LSCFO DP. The bias-field-dependent isothermal magnetic hysteresis loop exhibits large EB effect, which is easily explained using a disordered FM/AFM pinning boundary. The spin relaxation and spin dynamics have also been investigated from the time-dependent magnetization and training effect study of this system.

II. EXPERIMENTAL DETAILS

Polycrystalline LSCFO sample was synthesized by a conventional solid-state reaction method as described in Refs. [23,24]. The stoichiometric amount of La_2O_3 (4N), $SrCO_3$ (3N), Co_3O_4 (3N), and Fe_2O_3 (3N) powders have been mixed homogeneously and then calcined at 1000 °C for 10 h with several intermediate grindings in an acetone medium. Half of the calcined powders are then pressed into pellets for magnetic and relaxation measurements. Finally, the rest of the powders along with pellets are sintered at 1100 °C for 12 h. The crystallographic details of the polycrystalline bulk powder sample have been verified by a laboratory x-ray diffraction (XRD; Rigaku, SmartLab) apparatus with Cu-K_α source ($\lambda = 1.5405$ Å) at room temperature. The electronic structure of Co and Fe elements have been verified using x-ray photoelectron spectroscopy (XPS, PHI 5000 Versa Probe II Scanning) at room temperature. The temperature- and field-dependent magnetization measurements have been carried out in a physical property measurement system (Quantum Design, PPMS) in the temperature range of 5–350 K. To ensure complete demagnetization and thermal stabilization of the sample, the sample was heated to the paramagnetic (PM) state above the AFM transition temperature and then cooled to the desired temperature, followed by a five-minute wait time for each magnetization measurement. Using an oscillating field sequence, the trapped remanent field of the superconducting magnet was minimized to near zero value.

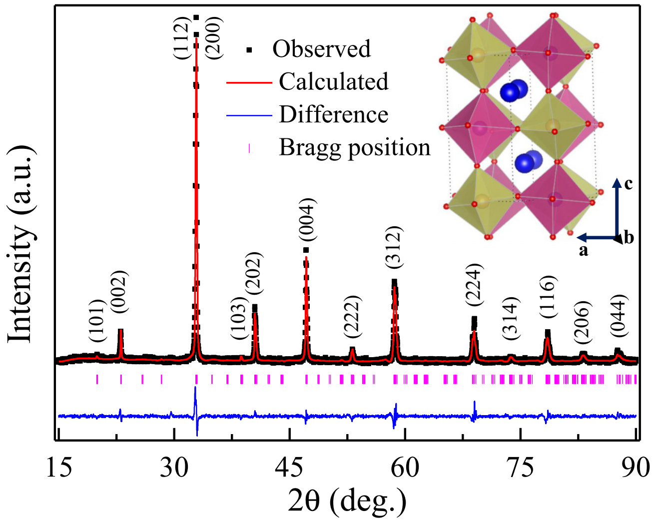

FIG. 1. Room-temperature powder x-ray diffraction pattern of LSCFO sample (dots) with the fitted curve (red line) and the difference (blue line), using Rietveld refinement. Inset shows a polyhedral picture of the unit cell of monoclinic LSCFO, where big balls (blue) and small balls (red) represent La/Sr and O atoms, respectively, while pink and yellow octahedra denote CoO_6 and FeO_6, respectively.

III. RESULTS AND DISCUSSION

A. Crystal structure

The room-temperature XRD pattern of LSCFO powder sample is employed to identify bulk phase, approximate compositions, and lattice parameters. Figure 1 shows the XRD pattern and Rietveld refinement results using FULLPROF SUITE for the 2θ range of 15° to 90°. The crystal structure of the powder LSCFO has been verified to possess monoclinic crystal symmetry with space group $P2_1/n$. No impurity peak is observed within the instrument's resolution limit, suggesting highly pure and single-phase material. The major reflections above the background level are indexed with monoclinic symmetry. The simulated structural parameters from the XRD pattern are presented in Table I. As a comparison, the XRD and neutron studies on parent compounds $LaCoO_3$ and $SrFeO_3$ have confirmed that the crystal structure of these two samples are rhombohedral (space group $R-3c$) and cubic (space group $Pm-3m$), respectively [21,24]. The mixture of $LaCoO_3$ and $SrFeO_3$ compounds transform the crystal structure of LSCFO to a low symmetry monoclinic (space group $P2_1/n$) due to the fractional replacement of the La site by Sr and the Co site by Fe or vice versa.

Inset of Fig. 1 exhibits local crystal structure of LSCFO, where Co and Fe are octahedrally coordinated with six oxygen atoms. The CoO_6 and FeO_6 corner-shared octahedra are located alternatively either at $2c$ ($\frac{1}{2}$, 0, 0) or $2d$ (0, $\frac{1}{2}$, 0) positions along the three crystallographic directions. Normally, the XRD peak around $2\theta = 20°$ is related to the Co and Fe ordering peak as suggested in Refs. [10–12]. In our sample, the observed intensity of this peak is very weak and almost screened by the background level with respect to the most intense peak at $2\theta = 33°$. This indicates the two CoO_6 and FeO_6 octahedra are not located alternately throughout the

TABLE I. Room-temperature lattice parameters, bond lengths (Å), and bond angles (°) for disorder LSCFO driven from Rietveld analysis of XRD data.

Lattice parameters							
a (Å)	b (Å)	c (Å)	α (°)	β (°)	γ (°)	V (Å^3)	χ^2
5.4410(2)	5.4537(5)	7.7079(3)	90.0	89.7658(9)	90.0	228.78	7.7
Bond length and bond angles							
La/Sr-O (Å)	Fe-O1 (Å)	Fe-O2 (Å)	Fe-O3 (Å)	Co-O1 (Å)	Co-O2 (Å)	Co-O3 (Å)	
2.4240	1.5656	1.9903	1.8688	2.2902	1.8705	2.0800	
	Fe-O1-Co (°)		Fe-O2-Co (°)		Fe-O3-Co (°)		
	177.509		171.977		154.517		

crystal, giving rise to partial ASD in the system. The weak peak around $2\theta = 20^\circ$ is observed due to very similar atomic absorption coefficient of the Co ($\sim$3240) and Fe ($\sim$2860) elements for Cu-K_α source. This evidence is not enough to probe completely the ASD in this DP system and hence further confirmation will be presented later from magnetization study.

The refined structural parameters in Table I and the local crystal structure (inset of Fig. 1) clearly indicate the bond length and bond angle are not particularly identical i.e., Co-O $\neq$ Fe-O and Co/Fe-O-Fe/Co $\neq$ 180°, which strongly indicates the presence of distorted crystal structure in the LSCFO system. Here, the Co-O/Fe-O bond length and Co/Fe-O-Fe/Co bond angle of LSCFO are different from the bond angle and bond lengths of an ordered DP compound at room temperature [27]. Generally, the disorder and distorted crystal structure in most of the perovskites influence the magnetic competitions and frustration in disordered systems [4–6]. In our disordered LSCFO system, a similar scenario could also be expected.

B. Isothermal magnetization and exchange bias study

To study the magnetic behavior, we have first carried out zero-field-cooled (ZFC) isothermal magnetization $M(H)$ measurements up to a field of $\pm$60 kOe at 5 K and 300 K. The $M(H)$ loops are shown in Fig. 2(a), where the inset shows the "virgin" curve from 0 to +60 kOe of ZFC $M(H)$ loop at 5 K. The ZFC $M(H)$ loop at 5 K possesses a well-defined saturationlike hysteresis having giant coercive field H_C of about 11.18 kOe and magnetic coercivity M_C of about 1.04 μ_B/f.u. The saturationlike hysteresis loop clearly demonstrates the mixture of FM and AFM phases in the low-temperature regime. The $M(H)$ versus H/T plot (not shown in this paper) at 5 K does not overlap at the origin ($H = 0$ and $M = 0$), which indicates that there is no superparamagnetic (SPM)-like signature and blocking of magnetic moments [28]. At 300 K, the $M(H)$ loop is a perfect PM straight line having zero H_C and M_C, confirming absence of magnetic impurities in this pure PM regime [29]. From the virgin $M(H)$ curve, we have calculated the M_S by fitting the high-magnetic-field part ($H \geqslant 20$ kOe) using the relation [30]

$$M(H) = M_S\left[1 - \frac{a}{H} - \frac{b}{H^2}\right] + cH, \tag{1}$$

where c is the high field differential susceptibility, a is linked with the structural defect and nonmagnetic inclusion of local magnetic moments, and b is related to magnetocrystalline anisotropy of the system. The estimated value of M_S for LSCFO [from inset of Fig. 2(a)] is $\sim$2.9 μ_B/f.u. As a comparison, the M_S value of a well-ordered La$_2$Co^{4+}Fe^{2+}O$_6$ structure should be 5.0 μ_B/f.u., since Fe^{2+} ($3d^6$: $t_{2g}^3 \uparrow$ $t_{2g}^1 \downarrow$ $e_g^2 \uparrow$) and Co^{4+} ($3d^5$: $t_{2g}^3 \uparrow$ $t_{2g}^2 \downarrow$ e_g^0) states contribute four and one unpaired electrons, respectively. Fe^{2+} and Co^{4+} are coupled ferromagnetically due to the superexchange interaction between the half-filled Fe^{2+} (d^6)-$t_{2g}^1 \downarrow$ state and empty Co^{4+} (d^5)-e_g^0 state via fully filled O-2p orbitals [31]. In our system, the observed low value of M_S indicates an existence of mixed valence states of Co (Co^{3+} and Co^{4+}) and Fe (Fe^{3+} and Fe^{4+}) due to Sr^{2+} doping at La^{3+} site [4].

Recently, conflicting results on the value of the Co valence state in LSCFO have been reported i.e., Co ($+2/+3$) by Tanwar *et al.* [32] and Co ($+3/+4$) by Pradheesh *et al.* [33]. From XPS analysis (not shown here), Co valence in our LSCFO sample is consistent with the results reported by Pradheesh *et al.* [33]. Theoretically, the spin-only moment for the intermediate spin state of Co (Co^{3+} and Co^{4+}) and high spin state of Fe (Fe^{3+} and Fe^{4+}) ions in ASD-free LSCFO crystal should be $\sim$6.3 μ_B/f.u. [21,31,34]. For the calculation, we have taken the ratio of Co^{3+} and Co^{4+} or Fe^{3+} and Fe^{4+} $\sim$1:1, which is consistent with our XPS results. This estimated theoretical value is not consistent with the observed experimental M_S value, which directly support the impact of ASD on the magnetic moment [10].

The ASD effect on magnetism can be easily visualized by replacing one Fe atom by one Co atom in an ordered crystal structure where CoO$_6$ and FeO$_6$ octahedra are periodically arranged in 3D. Figure 2(b) depicts the possible 2D arrangement of the crystal structure model of such an ASD in LSCFO system. In an ideal ordered DP structure like La$_2$CoFeO$_6$, each transition metal ion B (Co/Fe) is surrounded by six other transition metal ion B′ (Fe/Co) and exhibits FM correlation [31]. Interchanging the Co-Fe pair leads to a disordered structure. In this new disordered structure, one Co ion is surrounded by five Co ions and one Fe ion. A similar scenario is also observed for Fe ion. Hence, each disorder in doped LSCFO creates Co^{3+}–Co^{3+}, Co^{3+}–Co^{4+}, Co^{4+}–Co^{4+}, Fe^{3+}–Fe^{3+}, Fe^{3+}–Fe^{4+}, and Fe^{4+}–Fe^{4+} disorder ion pairs whereas each ordered arrangement creates Co^{3+}–Fe^{4+} and Co^{4+}–Fe^{3+}

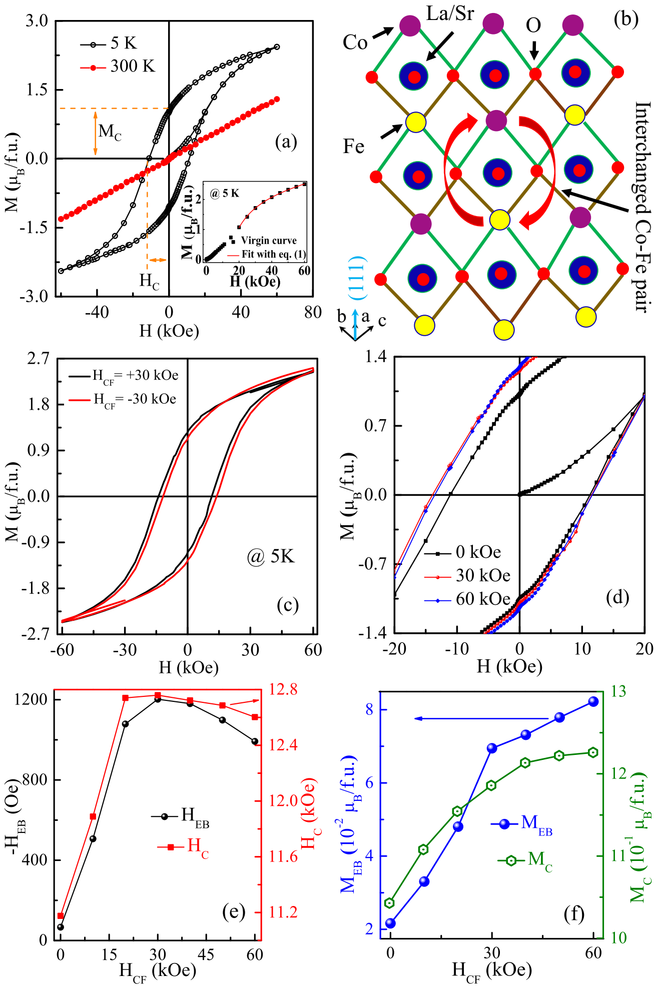

FIG. 2. (a) ZFC $M(H)$ isotherms in the range ±60 kOe at 5 K and 300 K. Inset shows the "virgin" $M(H)$ isotherm (black dots) taken from 5 K and the theoretical fit (red line) of Eq. (1) with $M_S = 2.9\ \mu_B$/f.u., $a = 11393.4$ Oe, $b = 4.03 \times 10^7$ (Oe)^2, and $c = 2.55 \times 10^{-6}\ \mu_B$/(f.u.-Oe) in the field range of 20 kOe $\leqslant$ H $\leqslant$ 60 kOe. (b) Two-dimensional schematic crystal-structure model for ASD LSCFO system. In this model, the atomic interchange between Co-Fe pair and degrees of antisite disorder are indicated. (c) The $M(H)$ isotherms measured at 5 K after cooling the sample from 300 K under +30 kOe (black curve) and −30 kOe (red curve) fields using two different protocols: (1) $H_{CF} = +30$ kOe: +30 kOe → +60 kOe → −60 kOe → +60 kOe and (2) $H_{CF} = -30$ kOe: −30 kOe → −60 kOe → +60 kOe → −60 kOe. (d) $M(H)$ isotherms in ZFC and FC modes at different cooling fields of 0, 30, and 60 kOe. (e) Cooling field dependent H_{EB} and H_C change at 5 K. (f) The variation of M_{EB} and M_C as a function of cooling fields.

order ion pairs. The disordered pairs are responsible for AFM ordering while ordered pairs are accountable for FM ordering. Each of these disordered interactions reduces the magnetic moment from the rest of the ordered part by 4.0, 3.31, 2.4, 8.3, 7.6, and 6.9 μ_B for Co^{3+}–Co^{3+}, Co^{3+}–Co^{4+}, Co^{4+}–Co^{4+}, Fe^{3+}–Fe^{3+}, Fe^{3+}–Fe^{4+}, and Fe^{4+}–Fe^{4+}, respectively [10]. Thus, total magnetic moment is significantly reduced by the ASD effect present in the system. The amount of the magnetic moment reduction is directly proportional to the amount of ASD present in the system[10]. This ASD is strongly responsible for the massive reduction of M_S, as a consequence of mixture of magnetic phases and magnetic frustration.

The presence of short-range ordering between the magnetic cations (Co and Fe) along with the presence of mixed valence states at low temperatures confirm the existence of magnetic anisotropy and frustration. The frustration originates at the pinning boundary of AFM and FM phases in LSCFO. There are several reports regarding the presence of EB in a similar type of magnetic oxides, having competing magnetic interaction and spin-torque anisotropy at the pining boundary after applying a cooling field [5,6,18]. Since the LSCFO system also has a low-temperature magnetic competition between FM and AFM phases, we have investigated the EB effect and spin relaxation dynamics in this frustrated system. The ZFC and field-cooled (FC) hysteresis loops at 5 K have been measured to understand the EB effect.

The minimum required anisotropy field H_A to eliminate minor loop effects can be evaluated using the fitting parameter b $(= 4K^2/15M_S^2)$ in Eq. (1) and $H_A = 2K/M_S$ [30]. The approximate estimated minimum H_A field required to completely flip the local spins linked to the EB effect is ∼24.6 kOe for this frustrated system, which is almost comparable with the value reported for single-layered $SrLaCo_{0.5}Mn_{0.5}O_4$ ($H_A = 20$ kOe) [35] and $LaMn_{0.7}Fe_{0.3}O_3$ ($H_A = 12.6$ kOe) [36]. In our system, all ZFC and FC hysteresis loop measurements have been carried out with $H_{\max} > \pm\ 30$ kOe field to avoid minor loop effects as shown in Figs. 2(a) and 2(c), respectively. It is clearly observed from Fig. 2(c) that the $M(H)$ loop measured with cooling field $(H_{CF}) = +30$ kOe is shifted toward negative field and positive magnetization axis with respect to the ZFC $M(H)$ loop. Whereas, the $M(H)$ loop measured with $H_{CF} = -30$ kOe is shifted systematically opposite to that with $H_{CF} = +30$ kOe. This observation confirms that significant shift of the hysteresis loop is due to EB effect.

For further confirmation of the EB effect and variation of EB parameters with the cooling field, we have investigated the FC hysteresis loop with the following protocol: cool the system from PM state to 5 K with different cooling fields ($H_{CF} = +10$, +20, +30, +40, +50, and +60 kOe) and then measure $M(H)$ loops with a scan field of ±60 kOe. The measured FC hysteresis loops are found to be shifted toward the negative field and positive magnetization axis, which is a clear sign of conventional EB effect [5,6]. Figure 2(d) shows the zoomed view of three selected hysteresis loops measured at 0, +30, and +60 kOe cooling fields. It is worthy to note that the LSCFO system does not exhibit hysteresis loop shift or spontaneous EB effect without any prebiasing magnetic field. The asymmetry of the FC hysteresis loop shift along both the field and magnetization axes can be traditionally defined as an EB field $[H_{EB} = \frac{H_{C1}+H_{C2}}{2}]$, coercive field $[H_C = \frac{|H_{C1}|+|H_{C2}|}{2}]$, and EB magnetization $[M_{EB} = \frac{M_{C1}+M_{C2}}{2}]$, magnetic coercivity $[M_C = \frac{|M_{C1}|+|M_{C2}|}{2}]$ where H_{C1} (H_{C2}) is left (right) coercive field and M_{C1} (M_{C2}) is the positive (negative) remanent magnetization [5,35,37]. The H_{CF} dependence of H_{EB} and H_C value are plotted in Fig. 2(e), where it is seen that the values of both H_{EB} and H_C rapidly increase with the increase of H_{CF} ($\leqslant$ 30 kOe) and then gradually decreases with further increase of H_{CF} (> 30 kOe). A similar trend in H_{EB} and H_C versus H_{CF} plots have also been observed in our earlier

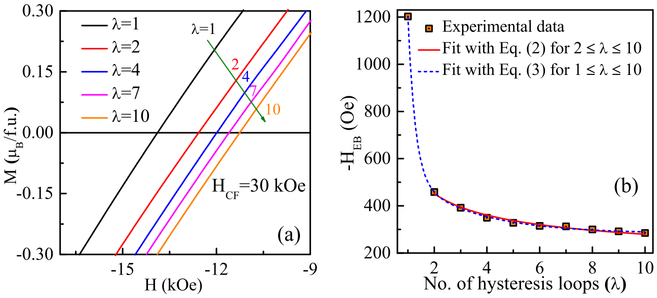

FIG. 3. (a) The zoomed view of the $M(H)$ isotherms in negative field axis measured at 5 K after +30 kOe cooling field, with ten continuous loops (magnetic training effect of EB). (b) The number of field cycle (λ) dependence of H_{EB} extracted from training effect at 5 K. The connecting lines are the best fitted by two different models mentioned in the text.

report on SG compound $La_{1.5}Ca_{0.5}CoMnO_6$ [5]. The observed maximum shift in H_{EB} and H_C are ~1.2 kOe and ~12.8 kOe, respectively, at $H_{CF} = 30$ kOe. On the other hand, Fig. 2(f) shows the change of M_{EB} and M_C with H_{CF}, which exhibits a slow increment above H_{CF}=30 kOe.

Magnetic training effect is a powerful and supportive technique used to confirm intrinsic EB phenomenon in the form of spin configurational relaxation for the minimization of spin torque in the pinning boundary [37]. At the pinning boundary, the magnetic anisotropy is assumed to be modified. It leads to gradual decrease of H_{EB} as the sample is repeatedly field cycled. For our LSCFO sample, ten successive $M(H)$ loops are measured at 5 K after $H_{CF} = +30$ kOe and the measuring field range is kept within ±60 kOe. Figure 3(a) shows the zoomed view of the $M(H)$ loops in the negative low field regime, where a few selective loops with index numbers (λ) of 1, 2, 4, 7, and 10 (for better observation) are shown. It is clearly seen from Fig. 3(b) that the magnetic training effect exists in the LSCFO sample as the value of H_{EB} is found to decrease monotonically with increasing λ. An almost similar dependence of H_{EB} with λ has been reported for other EB systems [5,35,37], where relaxation of interface spins at the FM/AFM heterostructure or local torque on AFM spins by the rotating FM magnetization reversal have been proposed as the explanation. In a frustrated LSCFO system, a huge change of H_{EB} (~ 58%) has been noticed in between the first ($\lambda = 1$) and second ($\lambda = 2$) cycles [shown in Fig. 3(b)]. On the other hand, only 14% change in H_{EB} is observed from second ($\lambda = 2$) to third ($\lambda = 3$) cycles. This huge decrease of H_{EB} suggests relaxorlike spin configuration at the pinning boundary, where the spins easily switch or flip with the external magnetic field [35,37]. Thus SG-like and/or frustrated spin configuration must be present at the pinning boundary in LSFCO. The variation of H_{EB} with λ can be described by a simple power law of the form [37]

$$H_{EB}(\lambda) - H_{EB}(\infty) \propto \frac{1}{\sqrt{\lambda}}, \tag{2}$$

where $H_{EB}(\infty)$ is the EB field at $\lambda \to \infty$. The solid line (red in the web version) in Fig. 3(b) shows the best fitted curve of H_{EB}, for $\lambda = 2$ to $\lambda = 10$. The parameter obtained from the best fit using Eq. (2) is $H_{EB}(\infty) = 240$ Oe. However, the above power law is invalid for $1 \leqslant \lambda < 2$ as it cannot describe the steep relaxation between $\lambda = 1$ and $\lambda = 2$. Here, the monotonic decrease of H_{EB} with each cycle is observed due to the asymmetric pinning boundary anisotropy. This magnetic anisotropy is strongly affected by the frozen, frustrated and rotating spins. Equation (2) can only describe energy dissipation of the AFM regions at the pinning interfaces [37]. However, it is impossible to demonstrate the change of H_{EB} with λ completely with this power law [Eq. (2)]. Recently, Mishra *et al.* [38] proposed a model to describe the training effect in a NiFe/IrMn bilayer system, where frustrated and rotating spins are present at the magnetically inhomogeneous FM/AFM interface. As our disordered LSCFO system shows EB below the frustrated and/or SG-like state, we can use the model proposed by Mishra *et al.* to describe the training effect. The mathematical expression for this proposed model is

$$H_{EB}(\lambda) - H_{EB}(\infty) = A_f \exp\left(-\frac{\lambda}{P_f}\right) + A_r \exp\left(-\frac{\lambda}{P_r}\right), \tag{3}$$

where A_f and P_f are the fitting parameters related to the change of the frozen spin configuration and A_r and P_r are the parameters related to the spin flipping of the frustrated spin component at the pinning boundary. It should be noted that A_f and A_r have the dimension of magnetic filed (Oe), whereas, P_f and P_r are dimensionless. From the excellent fit of H_{EB} data from $\lambda = 1$ to $\lambda = 10$ [shown in Fig. 3(b) by dashed blue line], the obtained parameters are $H_{EB}(\infty)$= 283 ± 6 Oe [almost equal to the estimated value obtained from Eq. (3)], $A_f = 25.4 \pm 10.1$ kOe, $P_f = 0.27 \pm 0.06$, $A_r = 346.9 \pm 72.9$ Oe, and $P_r = 2.5 \pm 0.4$. The relative ratio between P_f and P_r signifies the difference in the relaxation of both frozen and rotatable spin components. The observed value of P_r is much greater than that of P_f, which clearly indicates that the spin-flipping components relax (~7 times) faster than the frozen spin components at the pinning surface. A similar type of relaxor behavior has already been observed in various SG systems including our previous reports on SG compound of $La_{1.5}Ca_{0.5}CoMnO_6$ and $Sm_{1.5}Ca_{0.5}CoMnO_6$ [5,39].

C. Thermal variation of DC magnetization and spin glass

We now change our direction toward the ground-state behavior and the origin of EB effect in frustrated LSCFO systems. For this, we have carried out thermal variation of ZFC and FC DC magnetization $M(T)$ under 500 Oe DC magnetic field H_{DC} as shown in Fig. 4(a). There are three major highlights in this $M(T)$ curve: (1) the magnetization starts increasing from 268 K in both the ZFC magnetization (M_{ZFC}) and FC magnetization (M_{FC}) curves, (2) a significant slope change in the $M(T)$ near 200 K, and (3) a strong bifurcation between the M_{ZFC} and M_{FC} magnetization below the irreversibility temperature T_{irr}. These features are quite consistent with the $M(T)$ curves of SGs [6], cluster glass (CG) [4], SPMs [40], and other frustrated systems [35]. The ordering temperatures are estimated from the first derivative of M_{ZFC} (dM_{ZFC}/dT) [in Fig. 4(a)]. The observed first transition temperature T_N near 268 K is not very prominent due to the presence of more stable AFM phase due to $(Co/Fe)^{3+}$-O-$(Co/Fe)^{3+}$, $(Co/Fe)^{4+}$-O-$(Co/Fe)^{4+}$ and $(Co/Fe)^{4+}$-O-$(Co/Fe)^{3+}$ ordering. Interestingly, the FM phase arising from $(Co/Fe)^{3+}$-O-$(Fe/Co)^{3+}$

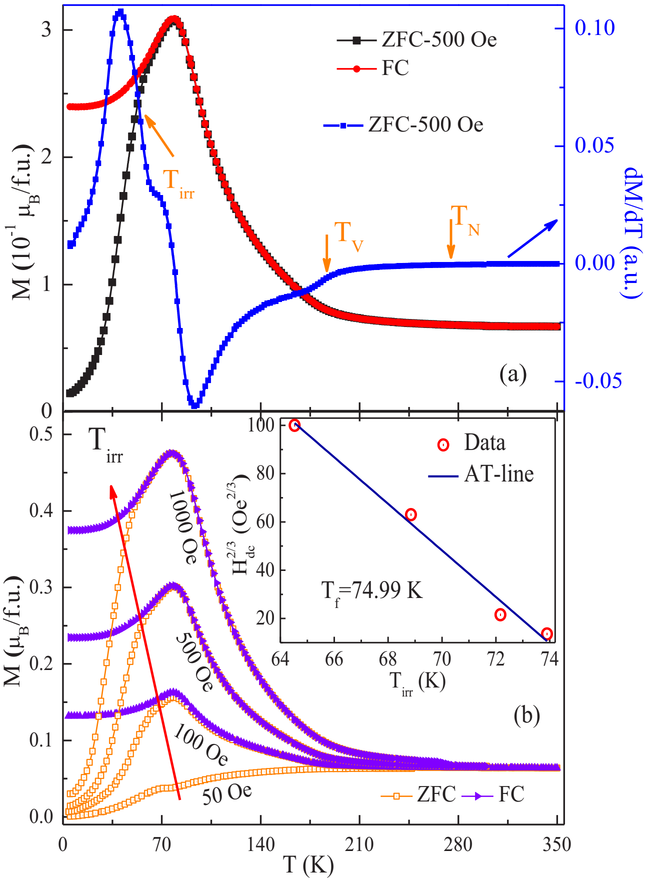

FIG. 4. (a) $M(T)$ curve of LSCFO measured at 500 Oe DC magnetic field H_{DC} under ZFC and FC mode and its temperature derivative dM_{ZFC}/dT as a function of temperature. (b) The DC $M(T)$ curves measured under various H_{DC} fields of 50, 100, 500, and 1000 Oe. Inset shows the corresponding plot of $H_{\mathrm{DC}}^{2/3}$ versus T_{irr} obtained from $M(T)$ curves and a linear fitting by De Almeida-Thouless (AT) line.

and $(\mathrm{Co/Fe})^{4+}$-O-$(\mathrm{Fe/Co})^{4+}$ coupling is also the second stable phase in the LSCFO system [13]. As a result, the magnetic moment increases monotonically with the decrease of temperature up to 80 K. A small peak near about 200 K (T_V) is visible in the dM_{ZFC}/dT curve due to the unit cell volume anomalies, which has already been established from temperature-dependent neutron and XRD analysis [33,41].

A strong magnetic irreversibility below 70 K is clearly visible in the M_{ZFC} and M_{FC} curves measured under various H_{DC} of 50, 100, 500, and 1000 Oe as shown in Fig. 4(b). It is seen that the T_{irr} is shifted toward the low temperature regime with the increase of H_{DC}. This shift can be assigned to a SG- or SPM-like behavior [4,5], but we have already ruled out SPM-like behavior from the low temperature $M(H)$ analysis. Thus, the SG-like frozen magnetic state most likely exists in the LSCFO system at low-temperature regime. The confirmation of the SG state comes from the FC and ZFC magnetization measurement at various DC fields. It is observed that T_{irr} shifts toward the low-temperature regime with the increase of H_{DC} fields, suggesting relaxation of frozen or SG state by an external field. The dependence of T_{irr} on the DC field is consistent with ordinary SG systems, and can be described with De Almeida-Thouless (AT) line, [4] i.e.,

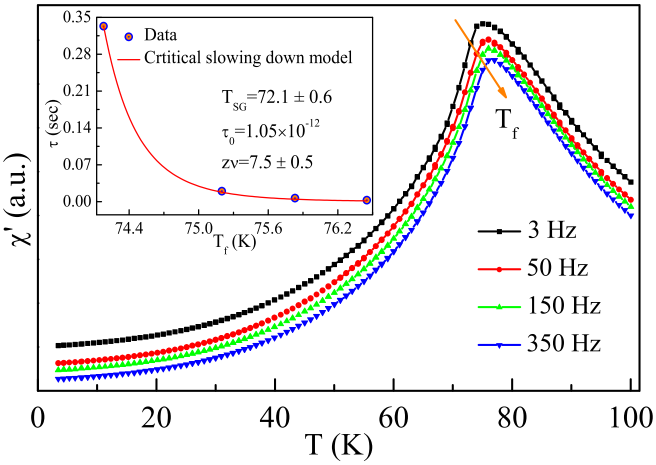

FIG. 5. Temperature-dependent real χ'(T) at different frequencies of 3, 50, 150, and 350 Hz. Inset shows relaxation time (τ) versus T_f at various f and the solid line (red) denotes a best fit to the critical slowing down model given in Eq. (5).

$$H_{\mathrm{DC}}(T_{\mathrm{irr}}) = \Delta J\left[1-\frac{T_{\mathrm{irr}}(H_{\mathrm{DC}})}{T_{\mathrm{SG}}}\right]^{\frac{3}{2}}, \qquad (4)$$

where T_{SG} is the SG freezing temperature at zero DC field and ΔJ is related to the exchange interaction. A satisfactory fit using Eq. (4) on the experimental data of $T_{\mathrm{irr}}(H_{\mathrm{DC}})$ versus $H_{\mathrm{DC}}(T_{\mathrm{irr}})$ supports the existence of SG behavior in LSCFO with a freezing temperature $T_{\mathrm{SG}} = 74.9$ K [inset of Fig. 4(b)]. A similar behavior has also been described in $\mathrm{La_{2/3}Sr_{1/3}MnO_3/STO}$ thin film in Ref. [42] and for Ni/NiO nanoparticles in Refs. [43,44], which is ascribed to the onset of freezing process of the frustrated spins.

D. AC magnetic susceptibility

To investigate further into the SG phase as well as dynamics of SG in LSCFO, AC susceptibility (real χ') measurements have been carried out in the temperature range of 5 to 100 K, with an AC field of 5 Oe and different frequencies (3 to 350 Hz), as shown in Fig. 5. It is clearly visible in Fig. 5 that the frequency-dependent maxima are shifted toward the higher temperature side with increasing frequency due to elongation of the action time-induced spin relaxation delay, which confirm a SG transition. As described in Ref. [4], the frequency-dependent peak shift parameter K for LSCFO is found to be ~0.022, which again rules out SPM and is consistent with the SG and CG behavior [45]. To distinguish between SG and CG nature in LSCFO, the frequency ($f = \frac{1}{\tau}$)-dependent peak shift temperature T_f in $\chi'(T)$ is fitted using the critical slowing down model [4]:

$$\tau = \tau_0\left(\frac{T_f - T_{\mathrm{SG}}}{T_{\mathrm{SG}}}\right)^{-z\nu}, \qquad (5)$$

The best fit, as displayed in the inset of Fig. 5, yields a microscopic spin relaxation time $\tau_0 = 1.05 \times 10^{-12}$ s, a dynamic critical exponent $z\nu = 7.5 \pm 0.5$, and a spin-freezing temperature $T_{\mathrm{SG}} = 72.1 \pm 0.6$ K. The results of τ_0 and $z\nu$ are comparable with a disordered SG system reported by Mydosh [46]. These results indicate that our system is a SG, not a CG system. The obtained T_{SG} is also in good agreement with that observed from the AT-line fit.

E. Features of spin glass and memory effect

Time-dependent magnetization measurements are complementary characteristics of SG phenomenon and magnetic memory effect exhibited by frustrated spin systems [4,43]. While measuring the magnetization as a function of time, magnetization is found to decrease or increase slowly depending on the magnetic field, which suggests relaxation of a frustrated spin system toward an equilibrium stable spin configuration [4,43]. To study the memory effect, temperature-dependent magnetization measurements have been performed in the FC mode with 100 Oe field by introducing intermediate stops at various temperatures T_{stop} of 210, 180, 80, 50, 30, and 10 K. The field is switched off at each T_{stop} for a relaxation period of 1 h. After reaching a low temperature (5 K), the system is heated from 5 K to 350 K without any T_{stop}. In the next step, FC magnetization measurement has been conducted for reference, without any stop. Figure 6(a) shows the magnetic field and temperature variations with time t during the memory effect experiments. Figure 6(b) shows the main experimental data for demonstrating the memory effect. The observed temperature-dependent FC magnetization curve clearly reveals that the system keeps measurement history in its memory in the low-temperature regime only. It is clearly seen from the inset of Fig. 6(b) that the system does not show any memory effect in the temperature range of 100 to 350 K as $\mathrm{FC_{stop}}$ magnetization and $\mathrm{FC_{heated}}$ (FCW) magnetization curves follow two different paths. This $M(T)$ behavior cannot support magnetic relaxation dynamics within 100–300 K. On the other hand, Fig. 6(c) and inset therein clearly manifest that the $\mathrm{FC_{stop}}$ magnetization shows lower values at each stop point and FCW magnetization follows $\mathrm{FC_{stop}}$ magnetization curve with prominent magnetization jumps around 10, 30, and 50 K. Here, the reference magnetization or FC reheated curve ($\mathrm{FCW_{ref}}$) and $\mathrm{FC_{stop}}$ magnetization curve do not coincide throughout the temperature regime, which is not very common for a pure SG system [47]. These results precisely confirm that LSCFO system has SG nature below 80 K along with frustrated magnetic phases.

For further confirmation of low temperature SG ordering and relaxation dynamics, time-dependent DC magnetic relaxation is examined well below the SG temperature, T_{SG} of LSCFO. The waiting time dependent slow relaxation has been investigated using the same experimental protocol as described in Refs. [29,48] and reproduces qualitatively identical results to support our SG claim. Figure 6(d) shows the waiting time ($t_W = 10^2$, 10^3 and 10^4 sec) dependent magnetization $M(t_W)$ as a function of time at 45 K (<74.9 K). The initial magnetic moment of each curve is different, which indirectly confirms the presence of a frustrated spin state at the low temperature regime. A popular stretched exponential model was employed to describe the t_W-dependent magnetization as a function of time [49],

$$M(t_W) = M_0 + M_{SG}\exp\left[-\left(\frac{t}{t_r}\right)^{1-n}\right], \tag{6}$$

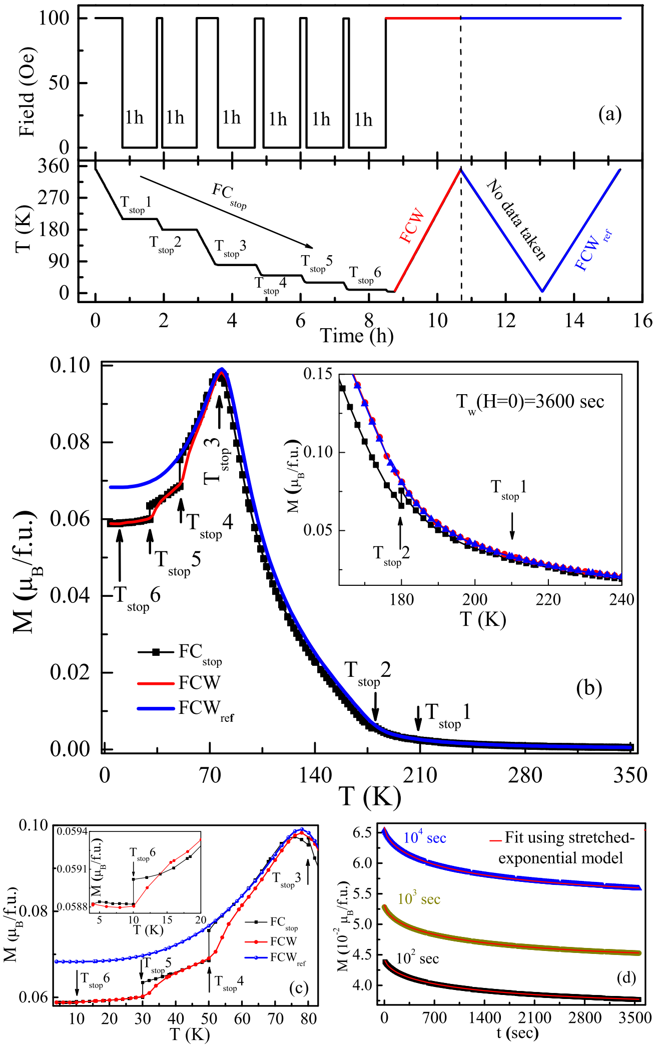

FIG. 6. (a) Raw data of magnetic field and temperature as a function of time (t) varied during memory effect experiments. (b) Temperature-dependent FC magnetization data recorded during the memory effect experiments. Inset shows zoomed view of FC magnetization versus temperature curves at high temperature regime. (c) and inset in (c) show the extended view of FC magnetization versus temperature curve in the low temperature regime. (d) Time dependence of isothermal (at 45 K) magnetization measured in the FC mode with an applied DC field of 100 Oe for different waiting times (t_W) of 10^2, 10^3, and 10^4 sec; the corresponding solid lines (red) are the best fit using the stretched exponential function described in Eq. (6).

where M_0 and M_{SG} are the moments of the FM and SG component, respectively, t_r is the mean relaxation time, and n ($0 < n < 1$) is the relaxation rate [4]. The parameters obtained from the best fit to $M(t_W)$ data are listed in Table II. The value of t_r (>10^3 sec) obtained from the fitting is a clear signature of SG state of LSCFO [4,49,50]. The nonzero values of M_0, M_{SG}, and n are also the signatures of coexisting SG and frustrated magnetic phase, driven by FM and AFM components in the relaxation process [29,49]. The presence of SG nature in this system is also consistent with the doped $\mathrm{LaCoO_3}$ [22,23].

TABLE II. Fitted parameters of the magnetic relaxations dynamics at 45 K for different wait times described in Fig. 6(d) using stretched exponential function.

t_W (sec)	M_0 (emu/gm)	M_g (emu/gm)	t_r (sec)	n
10^2	0.6938(6)	0.1473(1)	1824(13)	0.43(5)
10^3	0.5651(4)	0.1177(6)	1156(12)	0.41(4)
10^4	0.4637(4)	0.1057(7)	1220(14)	0.46(3)

F. Origin of spin glass and exchange bias

Below T_N, the short-range FM ordering competes with the AFM ordering in this DP system, which can be easily visualized from rising behavior of $M(T)$ curves [Fig. 4]. The coexistence of FM and AFM phases create a magnetic disorder, where FM and AFM boundary spins are highly frustrated in the low-temperature regime. These frustrated spins are responsible for the SG state below 80 K. All these frustrated SG spins are weakly coupled to the neighboring FM/AFM spins.

The EB effect has been extensively studied for SG and frustrated compounds with DP structure, where SG originates from the coexistence of short-range FM and AFM states [5,6,39]. In the present LSCFO system, similar kind of anisotropy in the pinning boundary between FM and AFM is accountable for such a large EB effect. Here, ASD-driven FM and AFM competition generates magnetic frustration which results in the SG behavior. In this frustrated ground state, the anisotropy direction at the FM and AFM pinning boundary is random and the net anisotropy is almost zero. Thus, ZFC EB is not seen in this DP system. The conventional EB is observed due to the nonzero unidirectional anisotropy at the FM and AFM pinning boundary. This frustrated ground state especially proposed from the model is suggested to explain conventional EB effect in $La_{1.5}Sr_{0.5}CoMnO_6$ [51], $La_{1.5}Ca_{0.5}CoMnO_6$ [5], and $LaFeO_3$ [52] polycrystalline perovskites. The variation of H_{EB} with the H_{CF} [Fig. 2(e)] is also well understood by considering this ground state. During cooling with a finite magnetic field, the SG spins and the nearest-neighbor spins are trying to align along H_{CF} direction. In $0 < H_{CF} \leqslant 30$ kOe range, the size as well as total magnetization of the FM domain is comparatively small and the unidirectional pinning boundary anisotropy is relatively large, which gives rise to the increase of H_{EB}. Upon further increase of H_{CF}, the number of FM domains and volume of these domains gradually dominate the magnetic structure. The large volume of FM ordered region decreases the unidirectional anisotropy at the FM/AFM pinning boundary. As a result, both H_{EB} and H_C decrease slowly after $H_{CF} > 30$ kOe. Interestingly, the slow increase of M_C and M_{EB} as a function of H_{CF} [Fig. 2(f)] also support our claim about the formation of large volume of FM ordering in this magnetic structure at $H_{CF} > 30$ kOe. Therefore, the ground-state magnetism of LSCFO is a superposition of three different magnetic phase contributions, i.e., AFM, SG phases, and linear field-dependent FM phase.

IV. CONCLUSIONS

Various experimental evidence confirms that fascinating multimagnetic states are present in this ASD LSCFO system. The LSCFO system exhibits near room-temperature AFM transition ($T_N \sim 268$ K). It also shows another low-temperature SG transition ($T_{SG} \sim 72.1$ K) due to the magnetic competition between short-range FM and AFM orderings. The pinning of the moments at the FM and AFM pinning boundary in the ground state is accountable for the EB effect with a large $H_{EB} \sim 1.2$ kOe and a giant $H_C \sim 12.8$ kOe. These large EB parameters and temperature-dependent magnetism in LSCFO systems makes it a promising candidate for spintronics applications. We suggest that large ASD is the core origin of all these interesting multifunctional features in the highly frustrated LSCFO system.

ACKNOWLEDGMENTS

We would like to acknowledge IIT Kanpur for financial assistance. Fruitful discussions with Pramod Ghising and Chanchal Sow are gratefully acknowledged. This work was partly supported by MEXT Element Strategy Initiative to Form Core Research Center (Grant No. JPMXP0112101001) and a Grant-in-Aid for Scientific Research (No. 18H03925) from the Japan Society for the Promotion of Science Foundation.

---

[1] D. Choudhury, P. Mandal, R. Mathieu, A. Hazarika, S. Rajan, A. Sundaresan, U. V. Waghmare, R. Knut, O. Karis, P. Nordblad, and D. D. Sarma, Phys. Rev. Lett. **108**, 127201 (2012).

[2] K. D. Chandrasekhar, A. K. Das, C. Mitra, and A. Venimadhav, J. Phys. Condens. Matter **24**, 495901 (2012).

[3] S. Baidya and T. Saha-Dasgupta, Phys. Rev. B **84**, 035131 (2011).

[4] R. C. Sahoo, S. K. Giri, D. Paladhi, A. Das, and T. K. Nath, J. Appl. Phys. **120**, 033906 (2016).

[5] R. Sahoo, D. Paladhi, P. Dasgupta, A. Poddar, R. Singh, A. Das, and T. Nath, J. Magn. Magn. Mater. **428**, 86 (2017).

[6] J. K. Murthy, K. D. Chandrasekhar, H. C. Wu, H. D. Yang, J. Y. Lin, and A. Venimadhav, J. Phys. Condens. Matter **28**, 086003 (2016).

[7] R. I. Dass and J. B. Goodenough, Phys. Rev. B **67**, 014401 (2003).

[8] K. Ueda, H. Tabata, and T. Kawai, Science **280**, 1064 (1998).

[9] K. Yoshimatsu, K. Nogami, K. Watarai, K. Horiba, H. Kumigashira, O. Sakata, T. Oshima, and A. Ohtomo, Phys. Rev. B **91**, 054421 (2015).

[10] S. Pal, Sharada Govinda, M. Goyal, S. Mukherjee, B. Pal, R. Saha, A. Sundaresan, S. Jana, O. Karis, J. W. Freeland, and D. D. Sarma, Phys. Rev. B **97**, 165137 (2018).

[11] C. Meneghini, S. Ray, F. Liscio, F. Bardelli, S. Mobilio, and D. D. Sarma, Phys. Rev. Lett. **103**, 046403 (2009).

[12] V. Shabadi, M. Major, P. Komissinskiy, M. Vafaee, A. Radetinac, M. Baghaie Yazdi, W. Donner, and L. Alff, J. Appl. Phys. **116**, 114901 (2014).

[13] G. R. Haripriya, C. M. N. Kumar, R. Pradheesh, L. M. Martinez, C. L. Saiz, S. R. Singamaneni, T. Chatterji, V. Sankaranarayanan, K. Sethupathi, B. Kiefer, and H. S. Nair, Phys. Rev. B **99**, 184411 (2019).

[14] X. Wang, Y. Sui, Y. Li, L. Li, X. Zhang, Y. Wang, Z. Liu, W. Su, and J. Tang, Appl. Phys. Lett. **95**, 252502 (2009).

[15] V. Kuncser, M. Valeanu, G. Schinteie, G. Filoti, I. Mustata, C. Lungu, A. Anghel, H. Chiriac, R. Vladoiu, and J. Bartolome, J. Magn. Magn. Mater. **320**, e226 (2008).

[16] J. Sort, J. Nogués, S. Suriñach, J. S. Muñoz, M. D. Baró, E. Chappel, F. Dupont, and G. Chouteau, Appl. Phys. Lett. **79**, 1142 (2001).

[17] A. López-Ortega, M. Estrader, G. Salazar-Alvarez, A. G. Roca, and J. Nogués, Phys. Rep. **553**, 1 (2015).

[18] J. Sort, S. Suriñach, J. S. Muñoz, M. D. Baró, J. Nogués, G. Chouteau, V. Skumryev, and G. C. Hadjipanayis, Phys. Rev. B **65**, 174420 (2002).

[19] J.-Q. Yan, J.-S. Zhou, and J. B. Goodenough, Phys. Rev. B **70**, 014402 (2004).

[20] C. Zobel, M. Kriener, D. Bruns, J. Baier, M. Grüninger, T. Lorenz, P. Reutler, and A. Revcolevschi, Phys. Rev. B **66**, 020402(R) (2002).

[21] P. G. Radaelli and S.-W. Cheong, Phys. Rev. B **66**, 094408 (2002).

[22] M. Zhuang, W. Zhang, and N. Ming, Phys. Rev. B **57**, 10705 (1998).

[23] K. Muta, Y. Kobayashi, and K. Asai, J. Phys. Soc. Jpn. **71**, 2784 (2002).

[24] S. Srinath, M. M. Kumar, M. L. Post, and H. Srikanth, Phys. Rev. B **72**, 054425 (2005).

[25] S. Ishiwata, M. Tokunaga, Y. Kaneko, D. Okuyama, Y. Tokunaga, S. Wakimoto, K. Kakurai, T. Arima, Y. Taguchi, and Y. Tokura, Phys. Rev. B **84**, 054427 (2011).

[26] M. Reehuis, C. Ulrich, A. Maljuk, C. Niedermayer, B. Ouladdiaf, A. Hoser, T. Hofmann, and B. Keimer, Phys. Rev. B **85**, 184109 (2012).

[27] T. K. Mandal and J. Gopalakrishnan, Chem. Mater. **17**, 2310 (2005).

[28] S. K. Giri and T. K. Nath, J. Nanosci. Nanotechnol. **12**, 7822 (2012).

[29] R. C. Sahoo, S. Das, S. K. Giri, D. Paladhi, and T. Nath, J. Magn. Magn. Mater. **469**, 161 (2019).

[30] H. S. Nair, T. Chatterji, and A. M. Strydom, Appl. Phys. Lett. **106**, 022407 (2015).

[31] H.-R. Fuh, K.-C. Weng, C.-R. Chang, and Y.-K. Wang, J. Appl. Phys. **117**, 17B902 (2015).

[32] K. Tanwar, D. S. Gyan, S. Bhattacharya, S. Vitta, A. Dwivedi, and T. Maiti, Phys. Rev. B **99**, 174105 (2019).

[33] R. Pradheesh, H. S. Nair, G. R. Haripriya, A. Senyshyn, T. Chatterji, V. Sankaranarayanan, and K. Sethupathi, J. Phys. Condens. Matter **29**, 095801 (2017).

[34] Y. Zhang, M. M. Schmitt, A. Mercy, J. Wang, and P. Ghosez, Phys. Rev. B **98**, 081108(R) (2018).

[35] R. R. Das, P. Parida, A. K. Bera, T. Chatterji, B. R. K. Nanda, and P. N. Santhosh, Phys. Rev. B **98**, 184417 (2018).

[36] M. Patra, M. Thakur, K. De, S. Majumdar, and S. Giri, J. Phys. Condens. Matter **21**, 078002 (2009).

[37] C. Binek, Phys. Rev. B **70**, 014421 (2004).

[38] S. K. Mishra, F. Radu, H. A. Dürr, and W. Eberhardt, Phys. Rev. Lett. **102**, 177208 (2009).

[39] S. K. Giri, R. C. Sahoo, P. Dasgupta, A. Poddar, and T. K. Nath, J. Phys. D **49**, 165002 (2016).

[40] S. Dhara, R. R. Chowdhury, and B. Bandyopadhyay, RSC Adv. **5**, 95695 (2015).

[41] T. Chatterji, B. Frick, M. Zamponi, M. Appel, H. S. Nair, R. Pradheesh, G. R. Hariprya, V. Sankaranarayanan, and K. Sethupathi, Phys. Rev. B **98**, 094429 (2018).

[42] B. Cui, C. Song, G. Y. Wang, H. J. Mao, F. Zeng, and F. Pan, Scientific Reports **3**, 2542 (2013).

[43] J.-Y. Ji, P.-H. Shih, T.-S. Chan, Y.-R. Ma, and S. Y. Wu, Nanoscale Res. Lett. **10**, 243 (2015).

[44] N. Rinaldi-Montes, P. Gorria, D. Martínez-Blanco, Z. Amghouz, A. B. Fuertes, L. Fernández Barquín, I. de Pedro, L. Olivi, and J. A. Blanco, J. Mater. Chem. C **3**, 5674 (2015).

[45] M. Giot, A. Pautrat, G. André, D. Saurel, M. Hervieu, and J. Rodriguez-Carvajal, Phys. Rev. B **77**, 134445 (2008).

[46] J. A. Mydosh, *Spin Glasses: An Experimental Introduction*, Vol. 125 (Taylor & Francies, London, 1993).

[47] S. K. Giri, A. Poddar, and T. K. Nath, J. Appl. Phys. **112**, 113903 (2012).

[48] S. Kundu and T. Nath, Philos. Mag. **93**, 2527 (2013).

[49] P. K. Pandey, R. J. Choudhary, and D. M. Phase, Appl. Phys. Lett. **103**, 132413 (2013).

[50] W. H. Meiklejohn and C. P. Bean, Phys. Rev. **105**, 904 (1957).

[51] J. Krishna Murthy and A. Venimadhav, Appl. Phys. Lett. **103**, 252410 (2013).

[52] H. Ahmadvand, H. Salamati, P. Kameli, A. Poddar, M. Acet, and K. Zakeri, J. Phys. D **43**, 245002 (2010).